International Symposium on Synergistic Effects of Materials and Processing (ISSEMP2006)
September 19, 2006 - Kumamoto University, Kumamoto, Japan

Material surface improvement for mercury target of spallation neutron source in J-PARC

M. Futakawa, Japan Atomic Energy Agency, Tokai-mura, Ibaraki-ken, futakawa.masatoshi@jaea.go.jp
T. Naoe, Ibaraki Univ., Hitachi-shi, Ibaraki-ken, naoe.takashi@jaea.go.jp
T. Wakui, Japan Atomic Energy Agency , Tokai-mura, Ibaraki-ken, wakui.takashi@jaea.go.jp
H. Kogawa, Japan Atomic Energy Agency, Tokai-mura, Ibaraki-ken, kogawa.hiroyuki@jaea.go.jp
H. Takeuchi, NDK, sagamihara-shi, Kanagawa-ken, takeuchi@ndkinc.co.jp

ABSTRACT

Liquid-mercury target systems for MW-class spallation neutron sources are being developed in the world. Proton beams will be used to induce the spalltion reaction. At the moment the proton beam hits the target, pressure waves are generated in the mercury because of the abrupt heat deposition. The pressure waves interact with the target vessel leading to negative pressure that may cause cavitation along to the vessel wall. Localized impacts by micro-jets and /or shock waves which are caused by cavitation bubble collapse impose pitting damage on the vessel wall. Bubble collapse behavior was observed by using a high-speed video camera, as well as simulated numerically. Localized impact was quantitatively estimated through comparison between numerical simulation and experiment. A novel surface treatment technique which consists of carburizing and nitriding processes was developed and the treatment condition was optimized to mitigate the pitting damage due to localized impacts. The surface improvement is effective to increase the lifetime of mercury target vessel.

INTRODUCTION

Mercury target system for spallation neutron sources, see in Fig.1, will be installed at MLF (Material Life Science Facility) in J-PARC (Japan Proton Accelerator Research Complex)[1,2]. At the moment proton beams bombard mercury targets, pressure waves are caused by rapidly thermal heat deposition in mercury and propagate into the target vessel wall[3]. The target wall is excited by the pressure waves to induce negative pressure along to the vessel wall. The negative pressure produces cavitation erosion on the vessel wall[4-7]. At MLF the proton beam hits the mercury target at 25 Hz. The cavitation erosion, therefore, becomes a crucial issue for structural integrity and lifetime estimation in the target[8]. MIMTM (Magnetic IMpact Tesing Machine); a pulse generator driven by electric magnetic force, was developed to systematically examine the cavitation erosion, so called pitting damage[9]. From the viewpoint of material approach to solve the issue, many kinds of conventional coatings and surface improvements were tried[10]. In general, harden surfaces have good resistance against pit formation[11]. On the other hand, interface strength between substrate and improved surface layer is affected by steep change of mechanical property between them. Among many kinds of surface improvements, plasma nitriding surface improvement showed relatively good performance to prevent from pitting damages. However, after million cycles of impacts the detached surface layers along to the interface between substrates and improved surface layers was observed. In order to optimize the thickness and hardness distribution of improved surface layer, numerical simulations was carried out as taking into account the localized impact due to mercury micro-jet impact based on experimentally observed bubble collapse behavior. In the presentation, the optimized surface layer which was improved by combination of plasma nitriding and carburizing processes to control a depth property distribution will be introduced.

EXPERIMENT

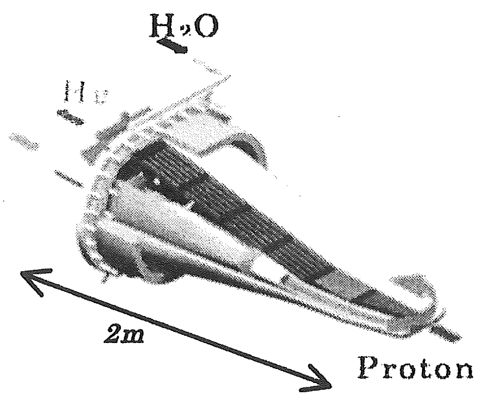

Figure 1 A MW-class mercury target in JSNS (Japan Spallation Neutron Source)

Figure 2 shows a mercury chamber and specimen in the MIMTM. The inner diameter and height are ϕ100 mm and 15 mm, respectively. The button-type specimen with ϕ15 mm diameter is fixed at the center of the disk plate. The impulsive pressure is imposed to the mercury through the disk plate driven with the striker controlled by the electromagnetic force. The magnitude of pressure is varied by the imposed power into the MIMTM. The morphology of pitting damage observed at the power of 560 W in the MIMTM is sufficiently equivalent to that in the on-beam tests using MW-class proton beams [9]. The repeated frequency of pulses is 25 Hz which is the same as that in JSNS. The morphology and depth profile of pits are observed using a laser microscope and an SEM.

Visualization of cavitation bubble formation was made by using a high-speed video camera (NAC MEMRECAM RX-6), whose frame rate was 20000 f/s. The bubble was formed on the interface between mercury and a glass window which was installed in a lid of the mercury chamber. A trigger signal was precisely controlled and input from the MIMTM to the camera at the onset of striker driving to investigate the relationship between time responses of imposed pressure in mercury and acceleration measured at the striker and the optical images of bubbles.

The materials of specimen are austenitic stainless steel type 316 and surface improved 316ss by plasma nitriding treatment, PN and combination of plasma

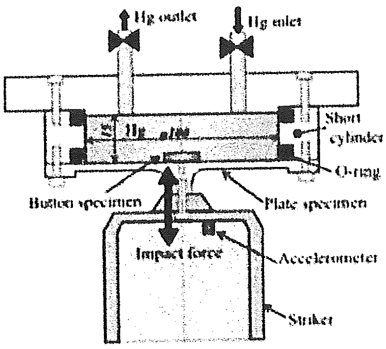

Figure 2 Mercury chamber and specimen in MIMTM

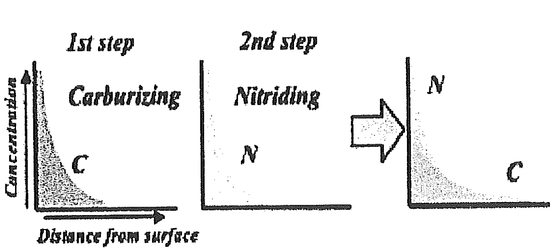

Figure 3 Concept of PCN surface treatment

carburizing PC and nitriding treatment PN, PCN. The conventional PN treatment was carried out at 673 K for 190 hr. The concept of PCN treatment was shown in Fig.3, consisting of two steps: in the first step the plasma carburizing treatment was carried out and then in the second step the plasma nitriding treatment to optimize the depth distribution of hardness. The trial PCNs were carried out in the following conditions: temperature from 673 to 723 K and period from 20 to 32 hr for carburizing, and 673 K and 80 to 190 hr for nitriding. Cross-sectional hardness distributions were measured using a micro-indention machine which can evaluate so-called universal hardness from measured indent load-depth curves [12].

IMPACT ANALYSIS

The pits are formed by the micro-bubble collapses that impose the localized impact on the solid/liquid interface by the micro-jets and/or shock waves collision against it. As assuming that the micro-jets are the most effective to form the pits, the analyses were carried out using an axisymmetrical model consisting of a spherical mercury droplet and a flat solid plate, as shown in Fig. 4. The mercury droplet was meshed in Eulerian coordinate and the solid plate in Lagurangian to be taken a large deformation into account by using AUTODYN-2D code [13]. The boundary conditions in the solid plate are free along to the collision surface and perfectly fixed conditions at the other ones. The following constitutive equations are used:

(1) For the droplet of mercury

Rankine-Hugoniot equation was applied to estimate the imposed pressure on the interface as follow;

$$p = p_H + \Gamma \rho (E - E_H) \quad , \qquad (1)$$

where Γ is Mie-Gruneisen coefficient, E internal energy, subscript H the value of Hugoniot-curve. Assuming that the internal energy is hardly varied by impact, the second term was ignored. p_H is given by

$$p_H = \frac{\rho_0 c_0 2\mu(1+\mu)}{\left[1-(s-1)\mu\right]^2}, \mu = \frac{\rho - \rho_0}{\rho}, \qquad (2)$$

where c_0 is sound velocity, ρ_0 initial density and s shock wave velocity parameter. For the mercury, c_0=1490 m/s, ρ_0=13.54x10^3 kg/m^3, s=2.047, and Γ=1.96 [13].

(2) For the solid plate

Johnson-Cook equation was applied to take the strain rate effect into account. Dynamic flow stress σ_{yd} is given by

$$\sigma_{y_d} = [A + B\varepsilon_p{}^n][1 + C\log\dot{\varepsilon}_p][1 - T_H{}^m], \quad T_H = (T - T_R)/(T_m - T_R) \qquad (3)$$

where ε_p is plastic strain, $\dot{\varepsilon}_p$ plastic strain rate, T temperature, T_R room temperature, T_m melting temperature, A static yield stress, B work hardening coefficient and n work hardening exponent, C strain rate work hardening coefficient, m softening coefficient. In the analysis, A=203 MPa, B=958 MPa, n=1, C=0 and m=1 for 316ss. The material properties; A and B for the PN and PCN treated surface layers were estimated by using the inverse analysis on the load/depth curves measured by nanoindentation technique that was developed by the authors [14,15].

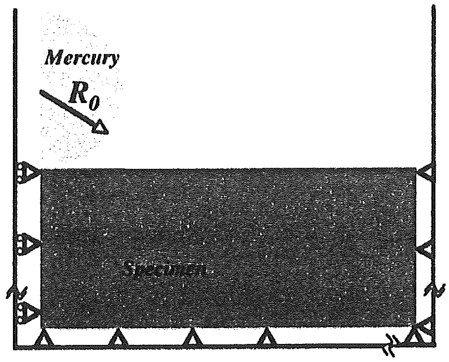

Figure 4 Simulation model for localized impact by micro-jet.

RESULTS AND DISCUSSION

Localized impact to form pits

Figure 5 shows the typical pictures taken by the high speed video camera, which caught the bubble collapse behavior with micro-jet impact. The micro-jet collided vertically against the glass window and spread out on the surface of glass window. The speed of mercury spreading *Vs* was estimated to be 200 to 300 m/s from the pictures. Figure 6 shows the results of numerical simulation on the micro-jet impact with the impact velocity *Vi* of 300 m/s, in which the micro-jet was assumed as a spherical droplet. The pit formation was hardly dependent on the shape of droplet[15]. *Vs* is dependent on *Vi* and almost equal to *Vi* in the range of *Vi* from 100 to 500 m/s. As a result, *Vi* was estimated to be 200 to 300 m/s, approximately.

Figure 7 shows stress distributions developed by the localized impact with *Vi*=300 m/s: (a) is as-received, (b) a homogeneous surface layer for the conventional PN surface layer, and (c) a gradient surface layer for the PCN one. It was clearly found that in (b)-case shear stresses are developed along to the interface between improved surface layer and substrate but the pit formation is sufficiently suppressed, on the other hand in (c)-case shear stresses on the interface are mitigated and pit formation is reduced as well. The PCN with gradient improved surface layer is expectable to suppress the pitting damage formation and

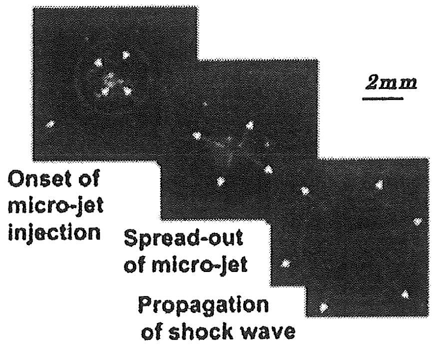

Figure 5 Typical pictures on bubble collapse taken by a high speed video camera.

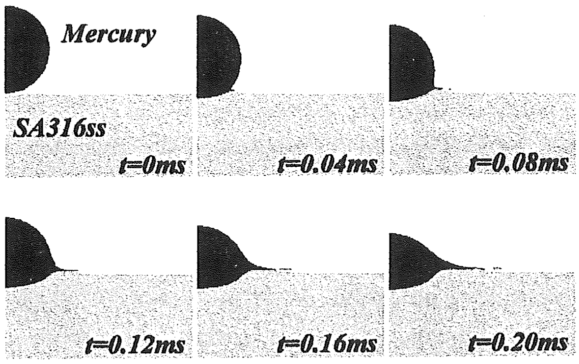

Figure 6 Numerical simulation on mercury micro-jet impact with *Vi* = 300 m/s.

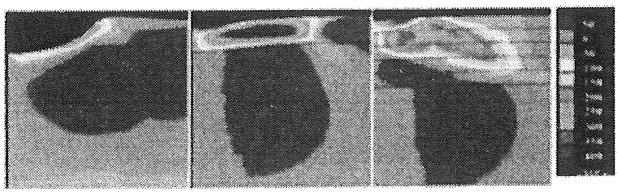

(a)As-received (b) Homogeneous surface layer (c) Gradient surface layer

Figure 7 Shear stress distribution developed by micro-jet impact with *Vi*=300m/s

survive under repeatedly localized impact for a certain period longer than the PN.

Improved surface layer

Figure 8 shows typical examples of cross-sectional hardness distributions in PC at 723 K for 20 hr and 673 K for 31.5 hr, and PN at 673 K for 80 hr and 190 hr, respectively. PN exhibits a steeper hardness distribution in the depth direction and a higher peak hardness than PC. The diffusion coefficients of PN and PC were evaluated by the following equation that was derived empirically by Hartis[16],

$$D=K^2/2t, \qquad (4)$$

where D is a diffusion coefficient, K thickness of improved surface layer and t treatment time. Table 1 shows the evaluated D values. The D value of carbon increased up to 3.6 times with 50 K increasing. The D value of carbon at 673 K is 2.6 times as much as that of nitrogen. These tendencies are the same one reported by Fast[17]. As taking into account the stress distribution by localized impact on the gradient improved surface layer shown in Fig.7 (b) and the treatment time efficiency as well as CrN and CrC formation to degrade corrosion resistance, we chose the following condition for the PCN treatment; PC at 723 K for 20 hr and PN at 673 K for 190 hr. Figure 9 shows a cross-sectional hardness distribution of the PCN treated surface layer. The carbon diffused in the first step was diffused even during the second step of PN treatment. The carbon diffused thickness calculated by using the D value in Table 1 got to be ca 50 μm, which is well agreement with the hardness distribution of PCN shown in Fig.9. In particular, a gradually inclined hardness distribution was obtained on the thickness from 20 to 40 μm. This hardness distribution is much suitable to prevent from pit formation and surface layer detachment as indicated through the numerical simulation seen in Fig. 7.

Table 1 Diffusion coefficients of each condition

Treatment	Temp. K	Time, hr	Diffusion coefficient, cm^2/s
PC	723	20	4.34×10^{-11}
PC	673	31.5	1.76×10^{-11}
PN	673	80	6.94×10^{-12}
PN	673	190	6.58×10^{-12}

Pitting damage

Figures 10 and 11 show 3D images and cross-sectional micrographs of damaged specimens of 316ss, PNed 316ss and PCNed 316ss after imposed impacts up to 10^7 cycles. Undamaged surfaces were not observed in 316ss and PNed one. In particular, PNed surface was partially detached from the substrate. In fact, homogeneous

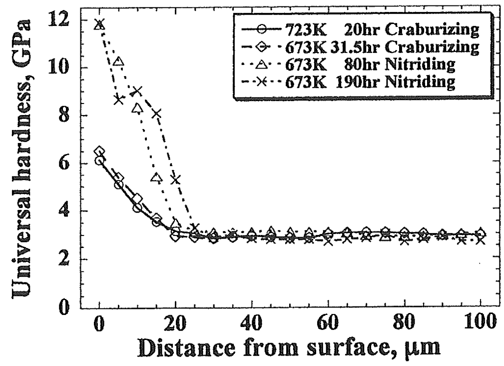

Figure 8 Typical examples of cross-sectional hardness distributions in PC and PN treated surface layers.

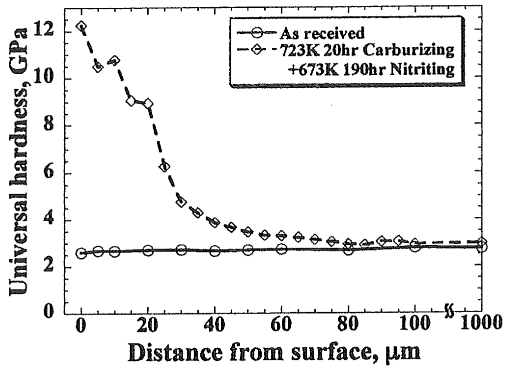

Figure 9 Cross-sectional hardness distribution in PCN treated surface layer.

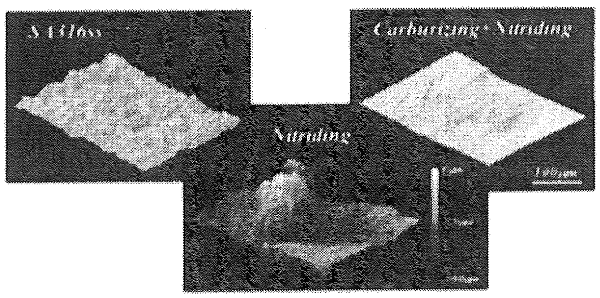

Figure 10 3D images of pitting damages in 316ss, PNed 316ss and PCNed 316ss.

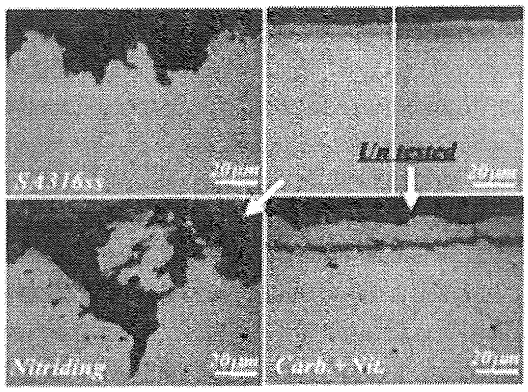

Figure 11 Cross-sectional micrographs of damaged specimens.

erosion already occurred after 10^6 impacts in 316ss [7,9]. On the other hand, the PCNed surface was hardly damaged and well protected the substrate from the pitting damage. As results, it was confirmed that the PCN surface treatment is very effective to mitigate the pitting damage of 316ss.

SUMMARY AND CONCLUDING REMARKS

Liquid-mercury target systems for MW-class spallation neutron sources are suffered from the pressure waves induced by high intense proton beam injection. The pressure wave propagation in target vessels results in cavitation along to the vessel wall. Localized impacts by micro-jet which is caused by cavitation bubble collapse impose pitting damage on the vessel wall. Bubble collapse behavior was observed by using a high-speed video camera, as well as simulated numerically. Localized impact was quantitatively estimated through comparison between numerical simulation and experiment. A novel surface treatment technique that consists of carburizing and nitriding processes was developed and the treatment condition was optimized to mitigate pitting damage due to localized impacts. The surface improvement is effective to increase the lifetime of mercury target vessel.

The surface treatment is also useful to reduce fatigue degradation because the target vessel is loaded by pressure waves at 25 Hz in J-PARC[18]. Furthermore, the effect of neutron and proton irradiations on material properties of improved surface layer should be considered[19]. These issues will be introduced in the presentation as well.

ACKNOWDGEMENT

This research is partly supported by a Grant-in-Aid in Scientific Research by the Japan Society for Promotion of Science, No. 16206097 and No. 17360085.

REFERENCES

[1] Nagamiya S., "Overview of the J-PARC Project", Neutron News, Vol. 16, No. 1 16(2005).
[2] Ikeda Y., "1-MW Pulse Spallation Neutron Source (JSNS) of J-PARC", ibid, 20(2005).
[3] Futakawa M., Kikuchi K., Conrad H., Stechemesser H., Pressure and stress waves in a spallation neutron source mercury target generated by high-power proton pulses, Nucl. Inst. Meth. in Phys. Res. A, 439,1-7(2000).
[4] Futakawa M., Kogawa H. and Hino R. ,Measurement of dynamic response of liquid metal subjected to uniaxial strain wave, J. Phys. IV France 10 Pr9-237-242(2000).
[5] Futakawa M., Kogawa K., Hino R., Date H. and Takeishi H., Erosion damage on solid boundaries in contact with liquid metals by impulsive pressure injection, Int J. Imp. Eng. 28 123-135 (2003).
[6] Haines J. R., Farrell K., Hunn J. D., Lousteau D. C., Mansur L. K., McManamy T. J., Pawel S. J., and Riemer B. W., Summary of Mercury Target Pitting Issue, SNS-101060100-TR0004(2002).
[7] Futakawa M., Naoe T., Tsai C.C, Kogawa H., Ishikura S., Ikeda Y., Soyama H., Date H., Pitting damage by pressure waves in a mecury target, Jour. Nucl. Mat. 343, 70-80, (2005).
[8] Futakawa M., Wakui T., Kogawa H., Ikeda Y., Pressure wave issues in high power mercury target, Nucl. Inst. Meth. in Phy.Res. A 562 676-679 (2006).
[9] Futakawa M., Naoe T., Kogawa H., Tsai C., Ikeda Y., Pitting damage formation up to over 10 million cycles -off-line test by MIMTM-, J. Nucl. Sci. Tech., 40, 895-904 (2003).
[10] Futakawa M., Naoe T., Kogawa H., Ishikura S., Date H., Hardening effect on impact erosion in interface between liquid and solid metals, J. Soc. Mat. Sci.,283-288 (2004) in Japanese.
[11] Garcia R., Hammitt F.G., Nystron, R.E.(1967), Correlation of cavitation damage with other material and fluid properties, ASTM STP 408, Am. Soc. Testing Mats., pp239-283.
[12] Futakawa M., Wakui T., Ioka I., and Eto M., Mechanical property evaluation of thin corroded surface layer of ceramic materials by microindentation technique, J. Euro. Ceram. Soc. 1135-1143 (2000).
[13] Futakawa M., Naoe T., Kogawa H., Date H., Ikeda Y., Micro-impact damage caused by mercury bubble collapse, JSME Int. Jour. A, 234-239 (2005).
[14] Futakawa M., Wakui T., Tanabe Y., Stress-strain relationship evaluation by load-depth curve obtained from indentation technique, 10th APCNDT, Brisbane (2001), Proc. CD-ROM.
[15] Futakawa M., Wakui T., Naoe T., and Ioka I., Inverse problem on indentation load and depth curve -Identification of material constants by using a spherical indenter- (in Japanese), J. JSEM, 50-56 (2004).
[16] Harris F.H., Metal progress, 265 (1943)
[17] Fast J.D., Verrijp M.B., Diffusion of nitrogen in iron, J. Iron Steel Inst. Vol. 183, 24-27 (1954).
[18] Futakawa M., Naoe T., Kogawa H., Teshigawara M., Ikeda Y., Fatigue strength degradation by pitting damage, Jour. Nucl. Mat. to be published.
[19] Naoe T., Futakawa M., Naito A., Kogawa H., Ikeda Y., Motohashi Y., Evaluation of mechanical properties and microstructure in ion-irradiated surface layer, JSME Int. Jour. A, 280-285 (2005).